Destruction of 0.1–3000-eV metastable hydrogen atoms in collisions with helium and argon

V. Dose and W. Hett
Physikalisches Institut der Universität Würzburg, 8700 Würzburg, Röntgenring 8, Germany

R. E. Olson, P. Pradel, F. Roussel, A. S. Schlachter, and G. Spiess
Service de Physique Atomique, Centre d'Etudes Nucléaires de Saclay, B.P. No. 2, 91190, Gif-sur-Yvette, France
(Received 5 June 1975)

Total deactivation cross sections for collisions of metastable H ($2\,^2S$) on He and Ar have been measured in the energy range 0.1–3000 eV. At low collision energies an apparatus designed to utilize time-of-flight techniques was used, while at the high energies an apparatus that employed beam-attenuation techniques was used. The cross sections are found to be on the order of 10^{-14} cm^2 at the lowest energies and decrease slowly to approximately 10^{-15} cm^2 at the highest energies. The experimental data were analyzed to obtain information about the difference in potential energies, $\Delta V(R)$, between the two $^2\Sigma$ molecular states arising from the $H(n=2)$ + He and Ar separated atoms. Our analysis also shows that the dominant deactivation mechanism of $H(2\,^2S)$ at energies less than 500 eV is excitation to $H(2\,^2P)$, which rapidly radiates to the ground state.

I. INTRODUCTION

Study of the destruction of hydrogen atoms in the metastable ($2\,^2S$) state by collisions with simple target atoms is of considerable interest in that the measured cross sections can be used to test various theoretical approaches to this problem. Such experimental results are now becoming available over a very wide range of energies of the incident metastable atom. In this paper we report the results of two independent experiments for $H(2\,^2S)$ and $D(2\,^2S)$ atoms incident on He and Ar targets, one experiment at thermal energies, the other in the energy range 75–3000 eV. We also present a theoretical calculation for collisional deexcitation, which links the two series of results. Preliminary experimental results (He target only) have been reported recently.[1,2]

The cross section we have measured is the total collisional destruction cross section σ_D, which results from the sum of three inelastic processes:

electron loss, σ_{m+}

$$H(2\,^2S)+X \rightarrow H^+ + e^- + [X]; \quad (1)$$

electron capture, σ_{m-}

$$H(2\,^2S)+X \rightarrow H^- + X^+; \quad (2)$$

collisional deexcitation, σ_{mg}

$$H(2\,^2S)+X \rightarrow H(n, l \neq 2s)+[X] \rightarrow H(1\,^2S)+[X], \quad (3)$$

where X is the target atom and $[X]$ indicates the possibility of target atom excitation.

Note that in process (3), deexcitation to the ground state may occur either directly or via another excited state; in our energy range the process is most likely to proceed via the adjacent $2P$ states. Thus

$$\sigma_D = \sigma_{m+} + \sigma_{m-} + \sigma_{mg}, \quad (4)$$

where σ_{mg} is the dominant cross section.

Previously reported measurements of σ_D are summarized in Table I. The present experiments were undertaken because of discrepancies in previously reported measurements, because of the improved accuracy and detail obtainable at thermal energies, and to fill in part of the gap at energies below 1 keV. Furthermore, the calculations in the present article allow us to consider the effects of elastic scattering at thermal energies, and to be sure that our results at higher energies are free from elastic scattering errors.

Various theoretical calculations on the above deactivation processes have been reported. The cross sections σ_D has been calculated by Byron and Gersten[11,12] from thermal energies (for He, Ne, Ar, Kr) to 250 eV (for He) by an impact-parameter approach using the interaction potentials derived from perturbation theory or a Breit-Fermi pseudopotential.

Byron, Krotkov, and Medeiros[13] have used an eikonal method to calculate σ_D for He in the energy range 0.5–5 keV. Slocomb, Miller, and Schaefer[14] have calculated σ_{mg} for He in the energy range 0.01–100 eV where they consider the $2s$-$2p$ transition as proceeding in the same manner as symmetric charge transfer. Levy[15] has utilized the first Born approximation with closure of the excited states to calculate collisional quenching for He, Ne, Ar, and Kr in the energy range 1 keV–1.6 MeV. Bell *et al.*[16] have also made a first-Born-approximation calculation of σ_{mg} in He for the energy range 5 keV–4 MeV.

TABLE I. Summary of reported measurements of σ_D in noble gasses.

Reference	Target	Energy range (KeV)
Pradel *et al.* 1974 (Ref. 1)	He	0.075–3
Dose and Hett 1974 (Ref. 2)	He	thermal
Kass and Williams 1971 (Ref. 3)	He	thermal
Kass and Williams 1973 (Ref. 4)	He, Ne, Ar, Kr	thermal
Comes and Wenning 1970 (Ref. 5)	He	thermal
Dose *et al.* 1969 (Ref. 6)	Ar	2–60
Gilbody *et al.* 1971 (Ref. 7)	He, Ne, Ar, Kr	10–30
Gilbody and Corr 1974 (Ref. 8)	He, Ar, Kr	5–500
Byron *et al.* 1970 (Ref. 9)	He	0.5–4.5
Krotkov *et al.* 1972 (Ref. 10)	He, Ar	0.25–30
Hughes and Berge 1974 (Ref. 11)	He, Ar	20–120
Present article	He, Ar	thermal, 0.075–3

In the calculations reported here, we have utilized our experimental data in the energy range $1 \lesssim E \lesssim 500$ eV and the theory presented by Slocomb *et al.*[14] to determine the difference between the potentials arising from $X+\mathrm{H}(2S)$ and $X+\mathrm{H}(2P)$, where X is He or Ar. The resulting difference potential is then compared to the *ab initio* results of Slocomb *et al.*[14] and Byron and Gersten.[12]

II. EXPERIMENTAL APPROACH: THERMAL ENERGIES

A. Apparatus

Figure 1 shows a schematic view of the apparatus employed at energies below 10 eV. Throughout this paper we shall call this low-energy region "thermal."

Metastable $\mathrm{H}(2\,^2S)$ atoms are produced by electron impact dissociative excitation of molecular hydrogen. The dissociation cell, where molecular hydrogen is bombarded with 60 eV electrons, has its center part free of electric fields in order to avoid immediate destruction of newly created $\mathrm{H}(2\,^2S)$ atoms. The exit channel of the dissociation cell together with the entrance channel of the target cell define a metastable atomic beam of rectangular shape, 1×4 mm. The beam passes through a quenching barrier which acts as a beam chopper. It is estimated that quenching voltages $\pm VQ$ of only ± 30 V are sufficient to destroy 99% of even the fastest metastable atoms in this experiment in the 2-mm-wide gap between the two quenching electrodes. In fact we were unable to detect any metastable atoms further downbeam with the quenching barrier closed.

Metastable atoms which have passed the quenching barrier when $VQ = 0$ traverse the target cell and enter a dc electric field through a copper mesh with 80% transparency and a 75-μm mesh width. Lyman-α radiation produced in this detection field is detected by a temperature-stabilized helium-iodine photon counter. The copper mesh separating the target region and the detection field is circular in shape with a diameter of 25 mm. This relatively

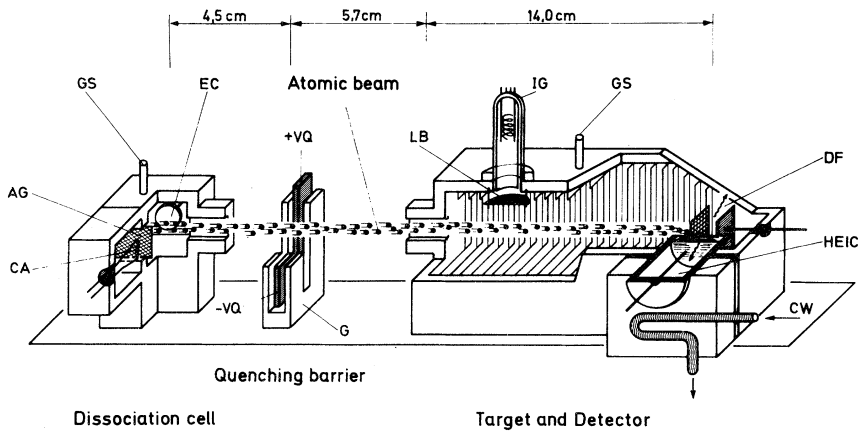

FIG. 1. Schematic view of the experimental arrangement for the thermal energies. Abbreviations have the following meaning: CA: cathode, AG: acceleration grid, GS: gas inlet, EC: electron collector, ±VQ: ground symmetric quenching voltage, G: grounded guard plates, IG: ionization gauge, LB: light trap, DF: detector field, HEIC: helium-iodine counter, CW: cooling water.

large angular acceptance of approximately 5° was believed to be sufficient to collect essentially all elastically scattered particles, so that beam attenuation as a function of target density would be unambiguously due to collisional quenching. This assumption is further discussed in Sec. IV.

The target density is measured with a triode-type ionization gauge. In order to obtain absolute cross sections we have calibrated the tube *in situ* before and after each cross-section measurement using gas-flow measurements. The conductance of the target entrance channel was determined separately by comparison with the conductance of a circular hole in a 0.1-mm wall, which can be accurately calculated for pressures in the molecular-flow region. The effective target length is 14 ± 0.5 cm, the uncertainty arising from a conservative estimate of the effective depth of the detection field and the effective length of the 10-mm-long target entrance channel. Since the accuracy of the ionization gauge calibration is found to be better than 2% for noble gases, the effective target thickness is known to better than 4% in this experiment.

The dissociation cell, quenching barrier, and target cell are mounted on a common aluminium bar and are housed in a 52-l vacuum chamber. This chamber is evacuated by a 250-mm-diam oil diffusion pump with a water-cooled baffle. The net pumping speed is ~1000 l/sec. The base pressure in the system is normally about 7×10^{-8} Torr and decreases to 1×10^{-8} Torr when liquid-nitrogen trapping is employed. The pressure rises up to 10^{-6} Torr during cross-section measurements. The optimum pressure in the dissociation cell is approximately 2×10^{-4} Torr. The maximum target pressure depends on the target species, and was chosen to produce a beam attenuation of a factor of 3 for medium projectile energies.

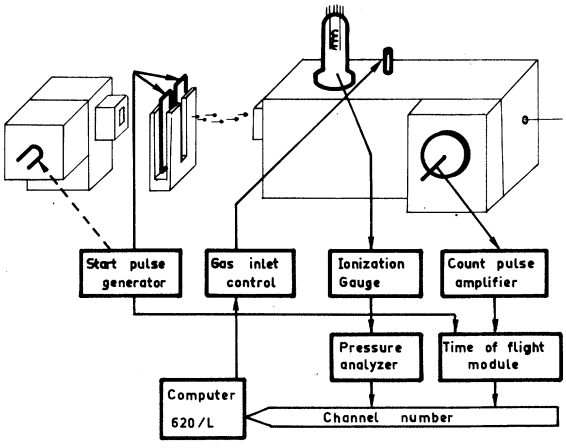

FIG. 2. Schematic view of the data-acquisition system used in the thermal-energy experiment.

B. Data acquisition

A block diagram of the data-acquisition system used in this experiment is shown in Fig. 2. The "start" pulse generator opens the quenching barrier for an interval of 1 μsec duration, thus forming a packet of metastable atoms. Simultaneously, a binary counter (time-of-flight module) is reset and subsequently advanced at a rate of 1 MHz. A metastable atom producing a signal in the iodine counter produces an interrupt signal for the computer. Upon the interrupt request, the computer reads the contents of the binary counter. This is interpreted as an address and the corresponding memory cell is incremented by 1.

Quenching cross sections are derived from time-of-flight (TOF) spectra taken at several different target thicknesses. In an early stage of this experiment the target pressure was varied by manual operation. In the present arrangement it is done automatically. A detailed description of the pressure modulation has been given elsewhere.[17] Briefly, the target pressure is varied continuously and periodically between prefixed minimum and maximum values at a rate of about 10 scans/h. The actual target density is derived from the current of an ionization gauge. The pressure analyzer digitizes this information. The information is then used to extend the channel address obtained from the TOF module. The pressure range is resolved in sixteen channels while 128 channels are used for the TOF analysis.

This system is not only convenient as it does not require much attention, but it is vital for lengthy measurements. Apparatus drifts which are slow compared to the time required for a single pressure scan become unimportant since they are averaged over, and consequently they do not affect the accuracy of a cross-section measurement.

C. Time-of-flight spectra

A typical TOF spectrum obtained from the dissociation of molecular hydrogen is shown in Fig. 3. Two maxima corresponding to velocities of 0.9×10^6 and 2.7×10^6 cm/sec are observed. Similar TOF distributions were obtained by Leventhal *et al.*[18] and Clampitt.[19] Misakian and Zorn[20] concluded from a detailed analysis of the threshold behavior and angular distribution of metastable dissociation products that slow metastables are produced partly by excitation of H_2 to repulsive regions of excited-state potential-energy curves and partly by excitation to bound states which then predissociate. Fast metastables, on the other hand, are due to dissociation of a doubly excited $^1\Pi_u$ state which behaves asymptotically as $H(2\,^2S) + H(2\,^2P)$.

For cross-section measurements it is highly desirable to close the gap between the two maxima in the TOF distribution. This can be done using a mixture of hydrogen and deuterium as a source gas. However, hydrogen and deuterium at the same velocity differ in energy by a factor of 2, and this could obscure finer details of the cross section as a function of energy. This point is discussed further in Sec. IV. Another way to achieve a less rapidly varying TOF distribution is to use a mixture of H_2 and CH_4 as a source gas. It is apparent from Fig. 3 that a substantial part of the $H(2\,^2S)$ TOF distribution obtained with CH_4 in the source falls in the minimum exhibited by the TOF distribution obtained from H_2.

D. Background

The metastable-atom signal is slightly distorted by background events. These can be measured separately with the quenching barrier continuously closed and everything else unchanged. Figure 4 shows a background TOF spectrum thus obtained. One may distinguish three contributions arising from different sources. The signal in the range $U1$ is due to direct excitation by ultraviolet radiation in the dissociation cell. This is by far the most important contribution. This signal is so large that dc operation of the dissociation cell was not possible and the electron gun was operated in a pulsed mode. However, since the rise time of the electron-gun acceleration voltage was rather poor, the exact timing for TOF analysis is still provided by the quenching barrier.

The signal in the range $U2$, which occurs at times up to 15 μsec after the electron gun is turned off, is due to Lyman-α radiation emitted by metastable atoms decaying at the closed quenching barrier. The solid line in Fig. 4 was calculated on the basis of this assumption using the known shape of the electron-gun pulse and the measured TOF distribution.

Finally, the small background in the region $U3$ is partly due to cosmic rays and another source that occurs only when the electron gun is "on." The latter source is not entirely understood. A possible explanation is that the primary events leading to these discharges in the helium-iodine counter are produced also in the ranges $U1$ and $U2$. An excessive delay between primary ionization and discharge in the counter would arise if negative-ion stripping in the counter had a finite probability. Since the drift times of negative iodine ions in the counter easily exceed the period for TOF analysis, this signal would appear uncorrelated as does $U3$.

E. Total destruction cross sections

If $N_K(p)$ is the number of acquired events in TOF channel K after suitable correction for background we then find $N_K(p)$ depends on the target pressure according to

$$N_K(p) = N_K^0 \exp[-nd\sigma_D(V_K)],$$

where n is the target number density, d is the effective target length, N_K^0 is the number of counts with $n=0$, and V_K is the projectile velocity corresponding to channel K. N_K^0 and σ_D were extracted from the experimental data using a least-squares

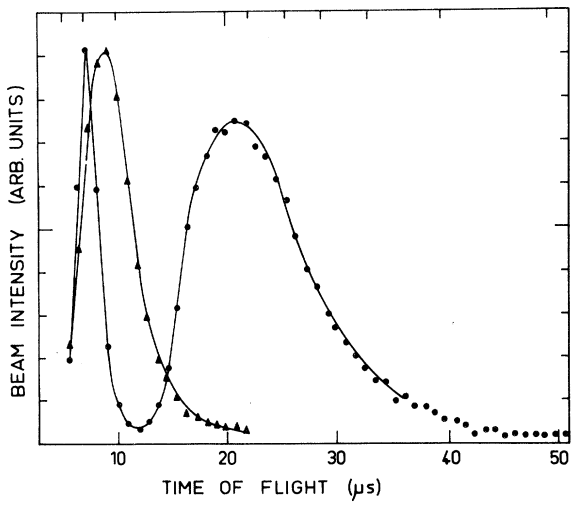

FIG. 3. Time-of-flight (TOF) spectra of the metastable hydrogen atoms. Solid dots give the TOF distribution obtained with H_2. Triangles refer to CH_4 and H_2.

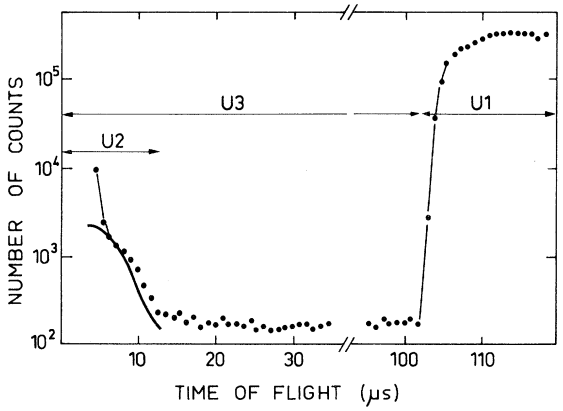

FIG. 4. Background spectrum taken with the quenching barrier closed. Contributions in the ranges $U1$, $U2$, $U3$, are due to different mechanisms described in the text. The solid curve in the left part of the figure was calculated assuming that the signal in $U2$ is due to Lyman-α radiation from metastable atoms decaying at the quenching barrier.

method. Error bars in Fig. 6 are random errors as obtained from the least-squares fit only. Absolute values are estimated to be accurate to 4% (see Sec. II A).

An uncertainty in the velocity V_K corresponding to TOF channel K (not drawn in the Fig. 6) arises from the finite TOF resolution and from an uncertainty in the flight path which adds a constant error of 2.5%. Finite time resolution is the dominating factor for fast metastables, and the error in the velocity assignment is approximately one-half the interval between successive velocities. For slow metastables the error in the flight path becomes important, and we obtain an accuracy of 3%. The two contributions are equal at $V_K = 10^6$ cm/sec.

III. EXPERIMENTAL APPROACH: HIGH ENERGY

A. Apparatus

Figure 5 shows the apparatus employed at energies above 75 eV. For the purpose of this paper we call this energy region "high." This apparatus has been previously described in detail.[21,22] It consists basically of a beam of fast H or D atoms in the $1\,^2S$ state with a large admixture in the metastable $2\,^2S$ state. The beam passes through a gas target, after which the H($2\,^2S$) atoms and the neutral H beam are detected. The total destruction cross section σ_D is determined by attenuation of the H($2\,^2S$) beam component and only relative measurements are necessary.

A proton or deuteron beam is extracted from a duoplasmatron source and is focused by an Einzel lens. The beam is magnetically mass analyzed and suitably collimated before entering a cell containing Cs vapor. The H^+ (D^+) beam, partially neutralized in the thin Cs target, contains H^+ and H^- ions, and H atoms in the $1\,^2S$ and $2\,^2S$ states. H atoms formed in the $2\,^2P$ states decay to the $1\,^2S$ state essentially immediately. Those formed in $2\,^2S$ state remain in that state, as the field-free lifetime is very long (0.14 sec). The beam emerging from the Cs target passes through a region where the ions are removed from the beam with a weak (<5 V/cm) transverse electric field, sufficient to remove all the ions from the beam, yet with minimal quenching (<2%) of the metastable H atoms. About 1 m downbeam from the Cs target is the gas-target cell where collisional quenching collisions are studied. The beam incident on this gas target contains essentially only atoms in the $1\,^2S$ and $2\,^2S$ states (between 25 and 50% in the $2\,^2S$ state[21-23]), as any H atoms in states with $3 \leq n \leq 6$, formed in the Cs target, would have time to decay to the $1S$ state.

The H^+ (D^+) and H^- (D^-) ions emerging from the gas cell can be analyzed by a 30° magnetic analyzer and measured with suppressed Faraday cups, symmetrically located about the beam axis. The neutral beam is measured with a detector that utilizes secondary-electron emission. The metastable fraction of the neutral component can be quenched by an electrostatic quadrupole. The resulting Lyman-α radiation is detected by a Bendix 762 channeltron which views the quenching region. The target gas cell has a 15 cm effective length (length of central part plus one end tube), an entrance aperture 5 mm in diameter, and an exit aperture 9 mm in diameter, in order to reduce beam losses by elastic scattering. The geometry of the target cell and of the quenching system defines an acceptance angle (half-angle) for the detection of H($2\,^2S$) atoms of 40 mrad. The base pressure in the vacuum system was 2×10^{-7} Torr.

B. Experimental method

The neutral beam contains not only metastable H (D) atoms, but also ground-state H (D) atoms. The ground-state component perturbs the measurements in that it produces metastable H atoms in the target-gas cell by collisional excitation:

$$H(1\,^2S) + X \rightarrow H(2\,^2S) + [X](\sigma_{gm}) , \qquad (5)$$

where X is the target atom.

For a given gas cell pressure p, we have compared the Lyman-α counting rates: $N(p)$, due to metastable H atoms remaining in the beam after

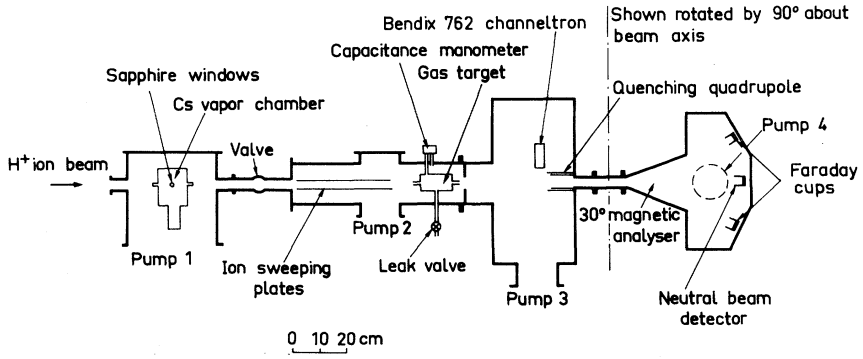

FIG. 5. Schematic view of the high-energy experimental apparatus. Chambers are drawn to scale. The ion source and the ion optic arrangement are not represented in the figure.

passage through the target, and $N'(p)$, due to metastable H atoms formed by reaction (5), when all the incident metastable atoms are prequenched. In the energy range studied, $N'(p)$ is typically no larger than 1% of $N(p)$; thus this contribution can be neglected. Furthermore, the values of σ_{gm} given by Birely and McNeal[24] and Orbeli *et al.*[25] are less than 2% of σ_D in the energy range 1–3 keV; thus the correction to σ_D is nearly negligible.

Then, for a given target thickness $\Pi = nd$ (where n is the density of the target and d is the effective target length), the metastable-atom intensity $I_m(\Pi)$ measured by the Lyman-α detector is given by

$$I_m(\Pi) = I_m(0)e^{-\sigma_D \Pi}, \tag{6}$$

where $I_m(0)$ is the metastable atom intensity without gas in the cell. Equation (6) neglects collisional excitation of ground-state H atoms since it is a small effect even in thick targets. The metastable atom intensity is measured with a Lyman-α detector which operates in a counting mode. The measured Lyman-α signal is the number of counts $N(\Pi)$ during a time period of 10 sec. In order to take into account fluctuations in the incident neutral beam during this period, we have normalized the Lyman-α signal to the measured neutral current (emitted secondary-electron current) down beam from the gas target during the same period (the neutral current is measured each second and the value recorded is the average value of the neutral current during the considered period of 10 sec).

We call $N(\Pi)$ the Lyman-α signal for a given target thickness Π, $I(\Pi)$ the neutral current recorded during the counting period, and $N(0)$, $I(0)$ the Lyman-α signal and the neutral current measured without gas in the target cell. The neutral current incident on the gas cell during the time that gas is in the cell cannot be measured and has to be estimated by a calculated value $I_{\mathrm{calc}}(0)$.

We can then write

$$N(\Pi)/I_{\mathrm{calc}}(0) = [N(0)/I(0)]e^{-\sigma_D \Pi}. \tag{7}$$

To calculate $I_{\mathrm{calc}}(0)$ we measured $N(\Pi)$, $I(\Pi)$ and $N(0)$, $I(0)$ alternately approximately 15 times each. We define an average neutral correction factor, which is

$$\langle R \rangle = \langle I(\Pi) \rangle / \langle I(0) \rangle . \tag{8}$$

This factor $\langle R \rangle$ is simply the sum of elastic and inelastic scattering processes which reduce the transmitted neutral current when gas is in the cell. If all elastic and inelastic cross sections were known, this factor $\langle R \rangle$ could, in principle, be calculated for our geometry.

We then estimate $I_{\mathrm{calc}}(0)$ by

$$I(\Pi)/I_{\mathrm{calc}}(0) = \langle R \rangle . \tag{9}$$

Averaging Eq. (7) over the set of data, we obtain

$$\langle R \rangle \frac{\langle N(\Pi) \rangle}{\langle I(\Pi) \rangle} = \frac{\langle N(0) \rangle}{\langle I(0) \rangle} e^{-\langle \sigma_D \rangle \Pi}, \tag{10}$$

which allows $\langle \sigma_D \rangle$ to be determined:

$$\langle \sigma_D \rangle = (1/\Pi) \ln(\langle F(0) \rangle / \langle F(\Pi) \rangle \langle R \rangle), \tag{11}$$

where

$$\langle F(0) \rangle = \langle N(0) \rangle / \langle I(0) \rangle$$

and

$$\langle F(\Pi) \rangle = \langle N(\Pi) \rangle / \langle I(\Pi) \rangle .$$

The error bars are calculated by taking into account the fluctuations in $F(0)$, $F(\Pi)$, $\langle R \rangle$, and Π and treating them as independent errors. $\Delta\Pi/\Pi$ has been taken to be 1% to take into account fluctuations in the gas pressure during the measurements. This does not include any possible systematic error in pressure measurement.

The pressure is measured by a capacitance manometer (M.K.S. Baratron type 170 M-7) with a special calibrated heating head having a full scale range of 1 Torr.[26] The error in the absolute pressure calibration is about 3%.[27] Typical target-gas pressure is 2.10^{-4} Torr, which gives an average attenuation of the Lyman-α signal of approximately 10%.[28] It was verified that the pressure in the chambers located before and after the target-gas cell remain lower than 1% of the pressure in the gas cell. The corresponding correction is lower than 3%.

Our measurements of σ_D (Fig. 6) are thus seen to be absolute, as there is no need to measure absolute currents (only relative "neutral currents") and no need to know the efficiency of our Lyman-α detector. The only absolute measurement required is of target thickness (thus pressure in the gas-target cell).

IV. THEORETICAL INTERPRETATION

A. Theoretical model and formalism

The interpretation of the experimental data has been made assuming that the relevant potential-energy curves are the two $^2\Sigma$ states arising from the H($n = 2$) + He or Ar combination. Within this assumption it then becomes relatively easy to calculate the inelastic cross section because the formalism reduces to the same equations as used in symmetric charge transfer, a good review of which is given by Mott and Massey.[29] Slocomb, Miller, and Schaefer[14] (SMS) have employed this very treatment in their prediction of the H($n = 2$) + He deactivation cross section.

In summary, the inelastic cross section is given

by the summation

$$Q=\frac{\Pi}{k^2}\sum_l (2l+1)\sin^2(\eta_l^+-\eta_l^-)\,, \tag{12}$$

where k is the wave number and $\eta_l^\pm$ are the elastic phase shifts for scattering on the two adiabatic potentials for a given angular momentum l. The difference in phases, $\Delta\eta_l=\eta_l^+-\eta_l^-$, may be accurately

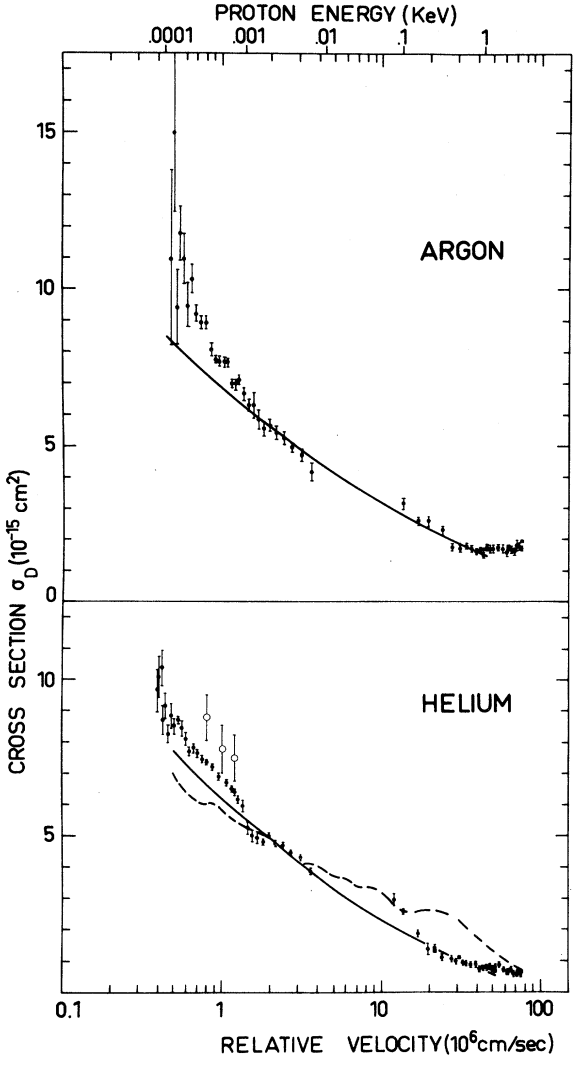

FIG. 6. Total destruction cross sections of $2\,^2S$ metastable hydrogen atoms in collisions with helium and argon. The bars indicate statistical errors. Solid circles: present work; open circles: R. S. Kass and W. L. Williams (Refs. 3 and 4) (1971–1973); solid squares: R. V. Krotkov *et al.* (Ref. 10) (1972); dashed line: theoretical calculation using the *ab initio* potential-energy curves of C. A. Slocomb *et al.* (Ref. 14); solid line: theoretical fits to the experimental data used to obtain the difference potentials.

calculated using the JWKB approximation, where the upper limit of integration is changed from $R_u=\infty$ to $\sim 20a_0$ for the H($n=2$)+He and Ar systems. In reality, $R_u\sim 20a_0$ is so large that the normal elastic phase shifts, where the integration is carried out to $R_u=\infty$, may be accurately employed at all but the very lowest collision energies, $E\lesssim 0.01$ eV. In this latter case, the impact parameters that contribute to the cross section become very large, and the elastic phase-shift approximation becomes invalid. The formalism also becomes invalid at very high energies, $E\gtrsim 500$ eV, where a two-state approximation obviously does not portray the many inelastic channels that are active in the deactivation of the H($2\,^2S$). However, for collision energies $0.01\lesssim E\lesssim 500$ eV, the above two-state approximation should be valid.

Since the difference potential $\Delta V(R)$ between the two $^2\Sigma$ states intimately related to the deactivation cross sections, it is possible to use the experimental data to derive information about $\Delta V(R)$. The analysis is considerably simplified if we assume a realistic functional form for $\Delta V(R)$, because then simple closed formulas may be used to determine the cross section. Although at very large internuclear separation $\Delta V(R)\sim R^{-7}$, it appears that, at the internuclear distances probed by the experiments, $4\lesssim R\lesssim 12a_0$, a simple exponential form is most realistic. The analysis can then be quickly carried out using the Firsov approximation[30] which has been shown to be quite accurate and easy to apply.[31] For

$$\Delta V(R)=Ae^{-R/B}\,, \tag{13}$$

it follows that

$$Q=\tfrac{1}{2}\Pi b_F^2\,, \tag{14}$$

where the Firsov impact parameter b_F is defined by

$$|\Delta\eta(b_F)|=\Pi^{-1}\,. \tag{15}$$

The difference in phase, in turn, is given in terms of the $K_1(X)$ modified Bessel functions by

$$\Delta\eta(b)=-(AB/\hbar v)\,\alpha K_1(\alpha)\,, \tag{16}$$

where

$$\alpha=b/B$$

is a dimensionless quantity. With the aid of a plot of α vs only $\alpha K_1(\alpha)$, the experimental totals may be rapidly analyzed to obtain the parameters A and B. A test of the validity of the exponential form chosen for $\Delta V(R)$ will be that a plot of Q vs $\ln v$ or $\ln E^{1/2}$ should yield approximately a straight line. The experimental cross sections may contain regular oscillatory structure, spaced at equal intervals of v^{-1}. This information can then be used

to extract additional information about $\Delta V(R)$.[31] Unfortunately, the data presented here do not display conclusive evidence of such structure.

B. H(n=2)+He system

For the H($n=2$)+He system, Slocomb *et al.*[14] have performed an elaborate calculation of the $^2\Sigma$ potential-energy curves. A Massey-Mohr approximation was then used to predict the inelastic cross sections. We have used Eq. (12) and the potentials of SMS to obtain the cross sections with improved accuracy. The results are presented in Fig. 6 along with the experimental data. The calculated cross section is found to have regular structure that is due to a change in inflection of the $\Delta V(R)$ around $R=3a_0$. The agreement is most encouraging, considering that the theoretical curve is an *ab initio* prediction of the cross section. At collision energies less than 1.0 eV, there appears to be an apparent disagreement between theory and experiment. However, this disagreement is due to the fact that, at very low collision energies, elastic scattering outside the detection angle of the experiment ($\theta_{1ab}\approx 5°$), substantially increases the experimental cross section.

We have calculated the elastic differential cross sections using the SMS potentials and the formulas of Olson and Mueller.[32] The differential cross sections were then integrated from $\theta_{1ab}=5°-180°$ to obtain the elastic scattering contribution. At 0.1 eV, the contribution was large,

$$Q_{el}(\theta_{1ab}\geq 5°)\approx 25\ \text{Å}^2$$

but luckily, the contribution decreases rapidly with increasing energy and becomes almost negligible at $E\approx 4$ eV.

The most serious disagreement between theory and experiment occurs at $100\lesssim E\lesssim 500$ eV. At these energies, deactivation of the H(2^2S) to the H(2^2P) is still the most important process. This argument is further supported by the experimental data that show that the production of negative or positive ions of H is negligible at these energies. Furthermore, additional deactivation processes other than the transfer of H(2^2S) to H(2^2P), such as to higher Rydberg levels of H, would be expected to increase, not decrease, the experimental cross section. Hence, we have used Eqs. (13)–(16) to predict an improved value of $\Delta V(R)$ that is compatible with the measurements. We find

$$\Delta V(R)=0.156e^{(-R/1.82)}\ \text{for}\ 4\leq R\leq 11a_0\,, \qquad (17)$$

where all quantities are in atomic units. The region of validity is determined from the internuclear separations most accurately probed by the 1–500-eV measurements.

The cross sections calculated using Eq. (17) for the difference potential are presented in Fig. 6. The difference potential is also compared in Fig. 7 to the $\Delta V(R)$ of SMS[14] and the long-range $\Delta V(R)\sim R^{-7}$ functional form given by Byron and Gersten.[12] We are in general agreement with the $\Delta V(R)$ of SMS, although at smaller internuclear separations, our $\Delta V(R)$ is approximately a factor of 2 smaller. This result would imply that the maximum at $R\approx 4a_0$ on the upper $^2\Sigma$ state of SMS could possibly be, in reality, lower by about 0.5 eV.

The experimental cross sections shown in Fig. 6 also display a slight hint of structure in the 100–500 eV energy range. The structure is predicted by the SMS potentials, so it is not unexpected. Also, as the calculations show, the amplitude of

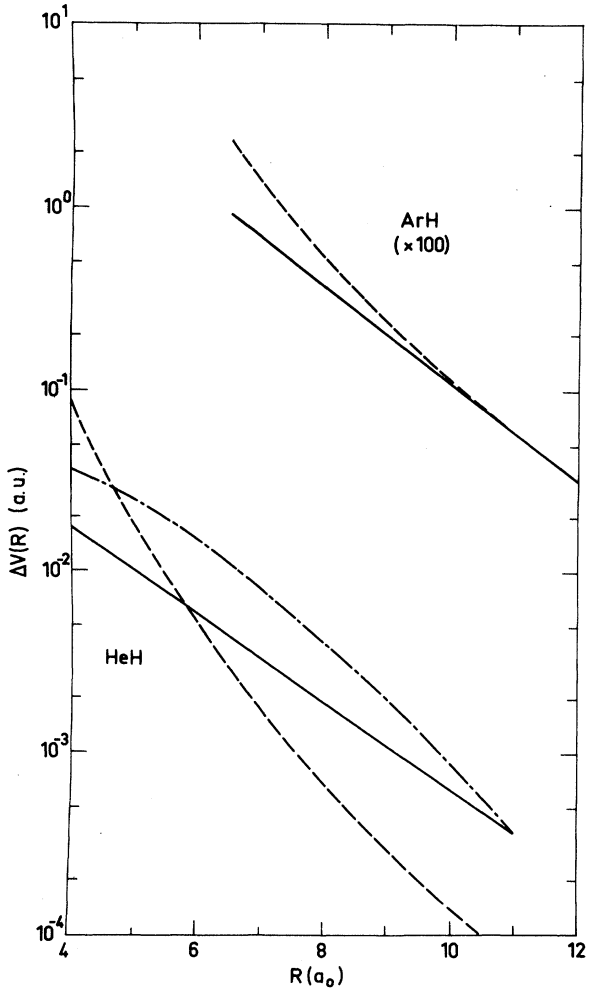

FIG. 7. Difference potential obtained from the experimental data: solid line; the difference potential of Slocomb *et al.* (Ref. 14): dash-dot line; the difference potentials of Byron and Gersten (Ref. 12): dash line.

the oscillations will be greatest, and hence most easily detected, at the higher energies.

C. H(n=2)+Ar system

A similar analysis has been performed on the cross sections for the H($n=2$)+Ar system. The difference potential obtained is

$$\Delta V(R) = 0.488 e^{(-R/1.64)}$$

in atomic units for $6.5 \leq R \leq 12 a_0$. (18)

The analysis utilized the experimental data between 1.0 and 400 eV. The cross section calculated using Eq. (18) is shown in Fig. 6, and the $\Delta V(R)$ is compared to the R^{-7} functional form of Byron and Gersten in Fig. 7. The agreement is encouraging.

We did not extend the analysis to energies less than 1.0 eV because of the problem that the experimental data probably contain an unknown amount of contribution from elastic scattering outside the laboratory acceptance angle. Since we do not have estimates for the individual potential curves of H($n=2$)+Ar, it is not possible to estimate the size of this cross section. At energies above 400 eV, transitions to higher Rydberg levels and negative- and positive-ion-formation processes become important. Hence, the analysis was not utilized on the cross section for $E > 400$ eV.

V. CONCLUSIONS

The total destruction cross section of $2\,^2S$ metastable hydrogen atoms in collision with helium and argon target atoms has been measured in the thermal-energy range and in the high-energy range using two independent methods. The accuracy of the two methods, except at very low energy, are of the same order of ±5% (statistical error). Although there is no energy overlap between the two sets of cross sections, the agreement in the extrapolated values was sufficient to eliminate large systematic errors and to employ a theoretical interpretation of the data that extended over almost five decades of energy. The high-energy data above 250 eV are very close to the previous measurements of Krotkov *et al.*[10]

For energies smaller than 500 eV, it was shown that the main destruction channel is the deexcitation of the $2\,^2S$ state of hydrogen via the adjacent $2\,^2P$ states. As the orbitals ($n=2$), of the hydrogen atom are hybridized by the perturbation due to the target atom, the $2S \rightarrow 2P$ transition was assumed to take place in the same manner as in the symmetric charge transfer where the theory is well known. Following this assumption the deexcitation cross section is essentially related to the difference between the two relevant potential-energy curves. Thus it was possible to derive accurate values of the potential difference by fitting calculated cross sections to the data for He and Ar.

In the case of the He-atom target, the difference potential is in general agreement with the previous *ab initio* calculation of Slocomb *et al.*,[14] but a significant discrepancy is noted in the internuclear separation range where the upper potential curve of Slocomb *et al.* exhibits a maximum ($R \approx 4a_0$). Our data would suggest that the size of this maximum could be over estimated by as much as 0.5 eV. However for more conclusive statement concerning such details in the potential-energy curves, certainly more experimental information is needed. Also, an oscillatory structure in the total cross section for He is predicted by the Slocomb *et al.* potentials. Although a slight hint for oscillatory behavior of the cross section is brought out by the present data, the structure is not clear enough to allow for any theoretical interpretation.

At energies higher than 500 eV, transitions to higher Rydberg levels and formation of negative and positive hydrogen ions become competitive processes so that the theoretical model that was developed is certainly not valid.

ACKNOWLEDGMENTS

The authors would like to thank Dr. Slocomb, Dr. Miller, and Dr. Schaefer for providing numerical data of their potential curves. We would like to thank Dr. C. Manus and Dr. G. Watel for their kind assistance. Part of this work has been supported financially by the Deutsche Forschungsgemeinschaft.

[1] P. Pradel, F. Roussel, A. S. Schlachter, G. Spiess, and A. Valance, Phys. Lett. 50A, 3 (1974).
[2] V. Dose and W. Hett, J. Phys. B 7, L79 (1974).
[3] R. S. Kass and W. L. Williams, Phys. Rev. Lett. 27, 473 (1971).
[4] R. S. Kass and W. L. Williams, Phys. Rev. A 7, 10 (1973).
[5] F. J. Comes and V. Wenning, Chem. Phys. Lett. 5, 199 (1970).
[6] V. Dose, V. Meyer, and M. Salzmann, J. Phys. B 2, 1357 (1969).
[7] H. B. Gilbody, R. Browning, R. M. Reynolds, and G. I. Riddell, J. Phys. B 4, 94 (1971).
[8] H. B. Gilbody and J. L. Corr, J. Phys. B 7, 1953 (1974).
[9] F. W. Byron, Jr., R. V. Krotkov, and J. A. Medeiros, Phys. Rev. Lett. 24, 83 (1970).
[10] R. V. Krotkov, F. W. Byron, Jr., J. A. Medeiros, and K. H. Yang, Phys. Rev. A 5, 2078 (1972).

[11]F. W. Byron, Jr., and J. I. Gersten, Phys. Rev. A 3, 620 (1971) [In Ref. 1 (Fig. 1) the theoretical calculation of Byron and Gersten is plotted as a solid line. The dotted line drawn in the text of the key is an error].
[12]F. W. Byron, Jr., and J. I. Gersten, Phys. Rev. Lett. 30, 115 (1973).
[13]F. W. Byron, Jr., R. V. Krotkov, and J. A. Medeiros, Phys. Rev. Lett. 24, 83 (1970).
[14]C. A. Slocomb, W. H. Miller, and H. F. Schaefer III, J. Chem. Phys. 55, 926 (1971).
[15]H. Levy II, Phys. Rev. A 3, 1987 (1971).
[16]K. L. Bell and A. E. Kingston, J. Phys. B 4, 162 (1971).
[17]V. Dose, W. Hett, U. Schmocker, and H. Windrich, Nucl. Instrum. Methods 124, 321 (1975).
[18]M. Leventhal, R. T. Robiscoe, and K. R. Lea, Phys. Rev. 158, 49 (1967).
[19]R. Clampitt, Phys. Lett. 28, A581 (1969); Entropie 30, 36 (1969); R. Clampitt and A. S. Newton, J. Chem. Phys. 50, 1997 (1969).
[20]M. Misakian and J. C. Zorn, Phys. Rev. Lett. 27, 174 (1971).
[21]P. Pradel, F. Roussel, A. S. Schlachter, G. Spiess, and A. Valance, Phys. Rev. A 10, 797 (1974).
[22]P. Pradel and F. Roussel, Nucl. Instrum. Methods 121, 111 (1974).
[23]Vu Ngoc Tuan, G. Gautherin, and A. S. Schlachter, Phys. Rev. A 9, 1242 (1974).
[24]J. H. Birely and R. J. McNeal, Phys. Rev. A 5, 257 (1972).
[25]A. L. Orbeli, E. P. Andreev, V. A. Ankudinov, and V. M. Dukelskii, Zh. Eksp. Teor. Fiz. 57, 108 (1969) [Sov. Phys.— JETP 30, 63 (1970)].
[26]Correction is made for thermal transpiration.
[27]We have verified our measurement of target thickness (effective target length, pressure) by comparing measured values of σ_{+0} with reported values.
[28]An attenuation of 10% is well within the limit of the "single-collision" region. However, we calculate σ_D using Eq. (6), i.e., an exponential, rather than the commonly used linear equation (the first term of the expansion), as, even for a 10% attenuation, this causes a 6% error in the cross section.
[29]N. F. Mott and H. S. W. Massey, *The Theory of Atomic Collisions* (Oxford U.P., New York, 1965), pp. 346–349.
[30]O. Firsov, Zh. Eksp. Teor. Fiz. 21, 1001 (1951).
[31]R. E. Olson, Phys. Rev. 187, 153 (1969).
[32]R. E. Olson and C. R. Mueller, J. Chem. Phys. 46, 3810 (1967).